Flutter Investigation of a Combat Aircraft with a Command and Stability Augmentation System

A. Lotze,* O. Sensburg,† and M. Kuhn‡
Messerschmitt-Bolkow-Blohm GmbH., Munich, Germany

Modern airplanes like the sweepable-wing combat aircraft Tornado are using sophisticated power control and automatic control systems, which basically are designed to maneuver the aircraft and to provide sufficient damping for the rigid body modes. Since the sensors are attached to a flexible structure, motions of the elastic aircraft also are picked up and may be modified by the system. In order to avoid instabilities it is necessary to predict the response of the airplane with the control system and to correlate with test data. An analytical approach for the complete system including unsteady aerodynamic forces is presented. The elastic structure is described by normal modes which have been modified by results of a ground resonance survey. Results of open- and closed-loop calculations are demonstrated in Nyquist and common flutter plots and compared with test data.

Introduction

THE purpose of this study is to develop and apply a reliable analytical procedure for determining the effects of a Command and Stability Augmentation System (CSAS) upon the flutter characteristics of a variable-sweep combat aircraft with stores. Such a study is necessitated because tactical requirements (weapon release, terrain following, etc.) led to the use of fast responding pressure feedback actuators capable of producing large forces at structural mode frequencies.

The airplane, being a combat aircraft, can carry numerous stores which vary widely in mass and inertia properties at four sweepable stations on the wing and under the fuselage. Consequently, a large number of configurations must be investigated. Thus, it is essential to have an analytical procedure that can predict the aeroelastic behavior of the aircraft reliably so that test work can be restricted to a few check points. To aid in developing a reliable procedure, the mathematical model of the aircraft is laid out in such a manner that it can be adjusted easily to match test data. The methods resulting from this CSAS structural interactions investigation have been applied successfully in active flutter suppression studies (Refs. 1 and 2).

The theoretical background of the method used is outlined in Ref. 3. A comprehensive description of the servo-aeroelastic problem is given in Ref. 4. This paper only deals with CSAS-structural mode interaction and rigid body flight mechanics investigations are not described. It is believed that these two tasks may be isolated when rigid body and elastic modes are separated by two octaves, a condition fulfilled by this aircraft.

Airplane Configuration and Primary Flight Control System

The airplane under study is the first operational aircraft featuring a triplex analog fly-by-wire control system, mechanical emergency control, and automatic stabilization (see Fig. 1). The primary flight control system provides pitch, roll, and yaw control by means of wing-mounted spoilers limited to low-speed conditions, an all-moving tailplane (taileron), and a conventional rudder.

Presented as Paper 75-1025 at the AIAA 1975 Aircraft Systems and Technology Meeting, Los Angeles, Calif., Aug. 4-7 1975; submitted Aug. 25, 1975; revision received Aug. 17, 1976.

Index categories: Structural Dynamic Analysis; Structural Stability Analysis

*Head of Aeroelasticity, Airplane Division.
† Head of Structural Dynamics, Airplane Division.
‡Principal Engineer Aeroelasticity, Airplane Division.

Equation of Coupled System Dynamics

Assuming linear behavior of the aircraft structure the flutter equation for the unaugmented system can be written generally in matrix notation as follows

$$m_r b_r^2 \begin{bmatrix} M_{qq} & M_{q\beta_0} \\ M_{\beta_0 q} & M_{\beta_0\beta_0} \end{bmatrix} \begin{Bmatrix} \ddot{q} \\ \ddot{\beta}_0 \end{Bmatrix} + \omega_r^2 m_r b_r^2 \begin{bmatrix} K_{qq}(1+ig) & 0 \\ 0 & K_{\beta_0\beta_0} \end{bmatrix} \begin{Bmatrix} q \\ \beta_0 \end{Bmatrix} + \frac{\rho}{2} A s \frac{b_r^2}{s^2} v^2 \begin{bmatrix} C_{qq} & C_{q\beta_0} \\ C_{\beta_0 q} & C_{\beta_0\beta_0} \end{bmatrix} \begin{Bmatrix} q \\ \beta_0 \end{Bmatrix} = \begin{Bmatrix} Q \end{Bmatrix} \tag{1}$$

where m_r, b_r, and ω_r are chosen reference mass, length, and frequency and M, K, and C are referred to as the generalized mass, stiffness, and aerodynamic matrices which are non-dimensional. The true airspeed v and the half span s of the

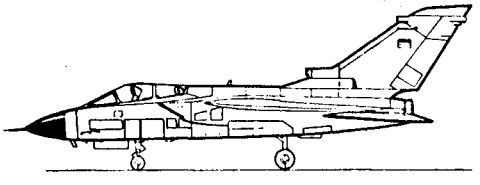

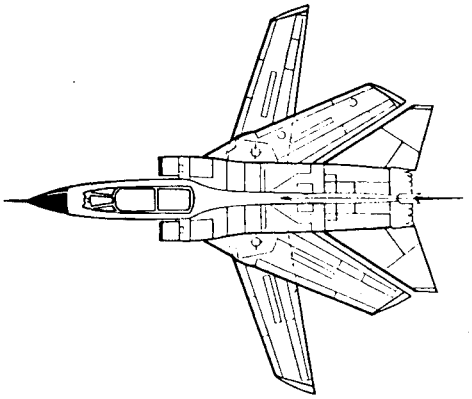

Fig. 1 Airplane view.

reference plane are used to form the reduced frequency $k=(\omega s)/v$. A is the area of reference plane and g is the structural damping of the elastic modes. The generalized forces Q are equal to zero for the conventional flutter problem. The generalized coordinate q describes the amplitude of the rigid body modes and the elastic airplane modes including elastic control surface modes for a system with actuators assumed to be rigid, whereas β_0 denotes the rotation of the rigid control surfaces according to the complex actuator stiffness represented by the impedance function of Eq. (2)

$$K_{\beta_0\beta_0}=K'_{\beta_0\beta_0}+iK''_{\beta_0\beta_0} \tag{2}$$

For the augmented aircraft the servo-induced control deflection $\Delta\beta$ has to be introduced as an additional degree of freedom for each control surface. The generalized forces Q generated by the servo-induced control deflections $\Delta\beta$ can be described as the right-hand term of Eq. (1) by

$$\left\{Q\right\}=-m_r b_r^2\begin{bmatrix}M_{q\Delta\beta}\\ M_{\beta_0\Delta\beta}\end{bmatrix}\left\{\Delta\ddot{\beta}\right\} -\frac{\rho}{2}As\frac{b_r^2}{s^2}v^2\begin{bmatrix}C_{q\Delta\beta}\\ C_{\beta_0\Delta\beta}\end{bmatrix}\left\{\Delta\beta\right\} \tag{3}$$

Assuming normalized rigid control surface mades β_0 and $\Delta\beta$, the rotation of each control surface can be superimposed by

$$\beta=\beta_0+\Delta\beta \tag{4}$$

Formulation of Closed-Loop Equations

For each control loop the motion of the structure picked up by the sensor can be expressed in terms of the modal displacements ϕ at the gyro station and the generalized coordinates $\dot{q}$ (q or $\ddot{q}$, if position or acceleration control is employed)

$$x_s=\left[\phi_{x_s}^{(q)}\right]\{\dot{q}\} \tag{5}$$

In accordance with the block diagram of Fig. 2 the relation between the servo-induced control surface deflections and the structural displacements sensed by the gyros are described by Eq. (6)

$$\{\Delta\beta\}=[F_{\text{Servo}}][F_{\text{CSAS}}][F_{\text{Sensor}}]\{x_s\} \tag{6}$$

where the transfer function of the CSAS also includes existing interfaces between the individual control loops.

Combining Eqs. (5) and (6), the control surface deflections $\Delta\beta$ can be expressed by the product of generalized coordinates q and the transfer function matrix R which contains the properties of interconnected control loops and the modal velocities (or displacements or accelerations) at the gyro stations.

$$\{\Delta\beta\}=[R]\{\dot{q}\} \tag{7}$$

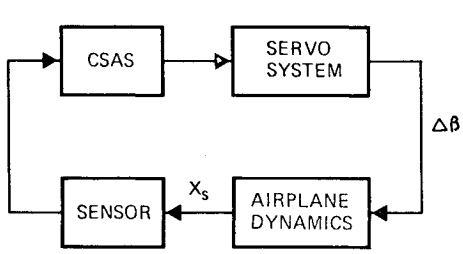

Fig. 2 Single-loop block diagram.

With the assumption of

$$q(t)=\hat{q}e^{pt} \text{ and } \Delta\beta(t)=\Delta\hat{\beta}e^{pt} \tag{8}$$

the equations can be transformed into the frequency domain. Introducing Eqs. (3) and (8) into Eq. (1) yields the eigenvalue problem for the augmented system.

$$\left(p^2 m_r b_r^2\begin{bmatrix}M_{qq} & M_{q\beta_0} & M_{q\Delta\beta}\\ M_{\beta_0 q} & M_{\beta_0\beta_0} & M_{\beta_0\Delta\beta}\end{bmatrix} +\omega_r^2 m_r b_r^2\begin{bmatrix}K_{qq}(q+ig) & 0 & 0\\ 0 & K_{\beta_0\beta_0} & 0\end{bmatrix} +\frac{\rho}{2}As\frac{b_r^2}{s^2}v^2\begin{bmatrix}C_{qq} & C_{q\beta_0} & C_{q\Delta\beta}\\ C_{\beta_0 q} & C_{\beta_0\beta_0} & C_{\beta_0\Delta\beta}\end{bmatrix}\right)\begin{Bmatrix}q\\ \beta_0\\ \Delta\beta\end{Bmatrix}=0 \tag{9}$$

$$\begin{bmatrix}R & 0 & -I\end{bmatrix}\begin{Bmatrix}q\\ \beta_0\\ \Delta\beta\end{Bmatrix}=0 \tag{10}$$

Equation (10) provides the necessary conditions for the added degree of freedom $\Delta\beta$. When the transfer function R and the impedance $K_{\beta_0\beta_0}$ are given as complex functions of the frequency, they can be treated by a similar procedure, as aerodynamic forces, usually are introduced into the flutter equation.

The iterative technique described in Ref. 5, known as the p-k method, was used, after some modifications, to solve the eigenvalue problem. Following this technique for a given airspeed v the expected frequency has to be extrapolated for each eigenmode and the frequency-dependent transfer functions and dynamic coefficients have to be interpolated. Introducing these coefficients into Eq. (9) and (10), the flutter problem can be solved for the eigenvalues

$$p=-\delta\omega\pm i\omega\sqrt{1-\delta^2} \qquad g\approx 2\zeta \qquad (\text{for } \zeta\ll 1) \tag{11}$$

This procedure has to be repeated until the difference between successively calculated eigenvalues is negligible. The method assumes that the damping in the characteristic mode is sufficiently low that the amplitudes of the aerodynamic forces are nearly constant. In each step of the process only the eigenvalue p corresponding to the trial value ω is computed.

Formulation of Open-Loop Equations

Figure 3 shows the block diagram for the open loop system which is cut off behind the sensor. The excitation is represented by a harmonic oscillating electrical input signal with constant amplitude for different frequencies. The deflection of the control surfaces for each single input can be calculated by

$$\{\Delta\beta\}=[F_{\text{Servo}}][F_{\text{CSAS}}]\{x_{\text{in}}\} \tag{12}$$

where the transfer functions F represent the complete control system including interfaces and only one element of the input vector x_{in} successively has a value unequal to zero. Having solved Eqs. (12) for the control surface deflection $\Delta\beta$, with consideration of

$$\Delta\ddot{\beta}=-\omega^2\Delta\beta \tag{13}$$

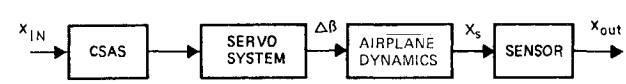

Fig. 3 Open-loop block diagram.

these deflections can be introduced into Eq. (3) to calculate the generalized forces Q.

For determination of the structural response the generalized forces, which are produced by the servo-induced control deflection $\Delta\beta$, are considered as right-hand terms of Eq. (1) which provides the generalized coordinates q. For stability considerations the output signal x_{out} defined in Fig. 3 resulting from the excitation signals can be displayed by Nyquist plots.

Idealization of the Structure

The clean aircraft was split up into four different substructures, namely, wing and center wing box, fuselage, tailplane, fin, and rudder. The wing was treated as a beam. For all of the other substructures influence coefficients were calculated with finite-element methods. Vibration modes of each substructure were produced and compared with and adjusted to available component tests. Rig tests were made to evaluate pylon stiffness for the wing-mounted stores. The stores were coupled to the wing with so-called discrete force modes (junction modes).[6]

The vibration modes of all substructures were used as branch modes and dynamically coupled together with rigid body modes to produce free-free total airplane vibration modes.[7,8] Twenty-one branch modes were used for clean aircraft calculations together with the rigid body modes plunge, pitch, fore and aft for the symmetrical case. Thirty-one branch modes and the rigid body modes roll, yaw, and side translation represented the antisymmetrical case.

The actuators were replaced by real springs having the same stiffnesses as the struts which represented the actuators in the airplane that was tested in the ground resonance test. The test airplane was suspended on soft springs to simulate the free-free condition. Calculated and measured vibration modes were compared and the mathematical model was adjusted to match the measured vibration modes. Because of the use of branch modes this was a relatively easy task. Having reached good correlation between calculated and measured modes, the real spring system which simulated the actuator stiffnesses was replaced by measured actuator impedance functions.

CSAS Defintion

A block diagram of the fully operative CSAS is shown in Fig. 4. The possible implementation of a structural filter must be provided in the design of the CSAS. Development work including tests should be done with a transfer function of unity for structural filters. All of the blocks in the diagram can be represented by linear transfer functions in the analysis. The actuator dynamics are highly nonlinear depending on preloading, amplitudes, input, and service conditions. One must be sure, therefore, that the transfer function of the worst possible case is introduced into the analysis.

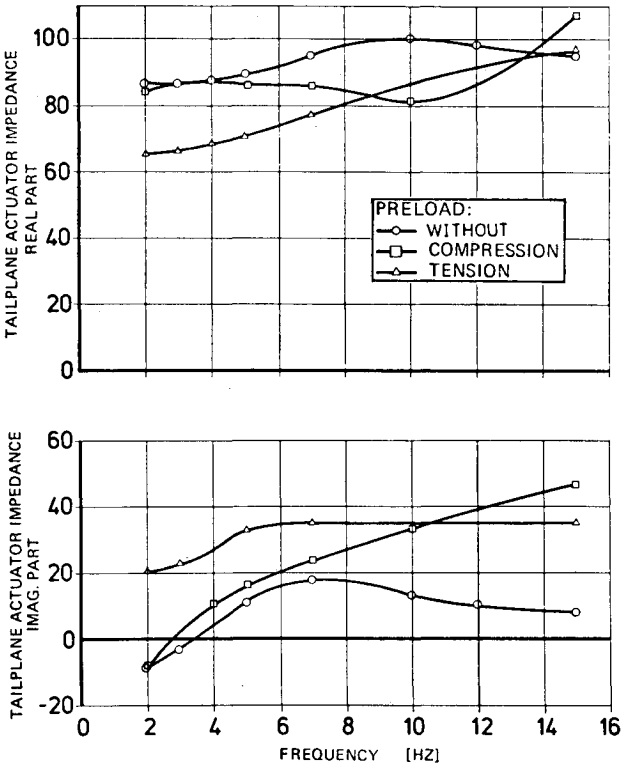

Fig. 5 Measured impedance-function of the tailplane actuator for various preloads.

Actuator Frequency Response and Impedance

Whereas transfer functions of all of the electrical blocks in the CSAS can be predicted analytically with sufficient accuracy, the actuator impedance and frequency response functions must be measured. These are very costly and time-consumming procedures considering the vast amount of variables that must be covered.

In Fig. 5 the variation of the taileron actuator impedance function with preload is shown. There are considerable differences in the functions that must be evaluated by the analyst. The large variation of taileron actuator transfer function with different input amplitudes is presented in Fig. 6. The transfer function shown includes the influence of a lag filter which was implemented into the taileron actuator circuit. Because of the actuator pressure feedback system which is electrically connected this easily could be accomplished. In addition to the structural mode filter, this filter increases attentuation at higher frequencies considerably, thus helping to suppress interaction with higher-frequency elastic modes.

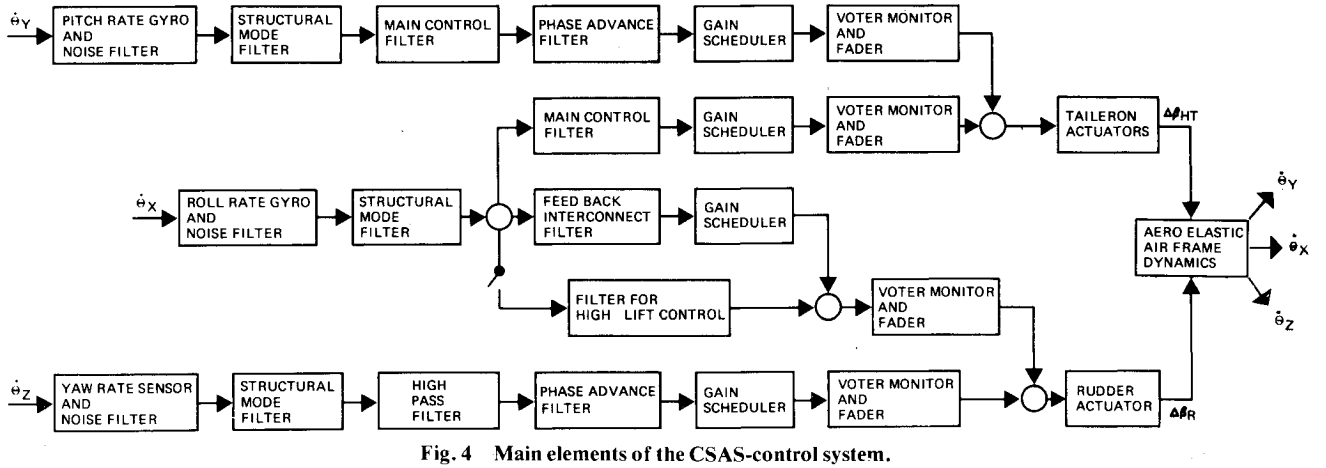

Fig. 4 Main elements of the CSAS-control system.

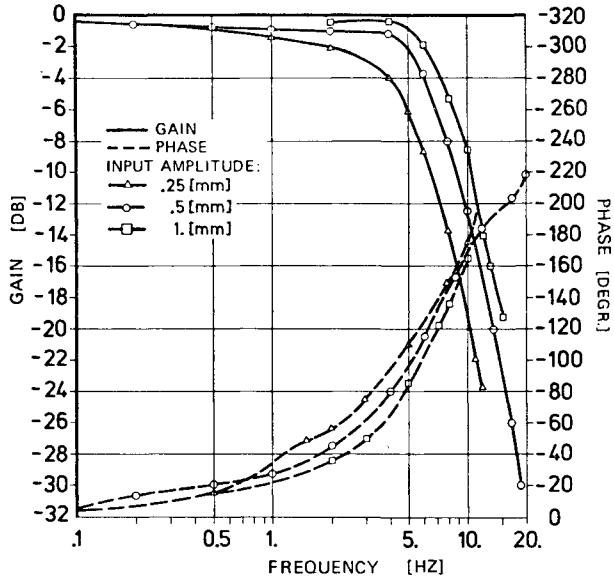

Fig. 6 Measured response function of the tailplane actuator for various input amplitudes.

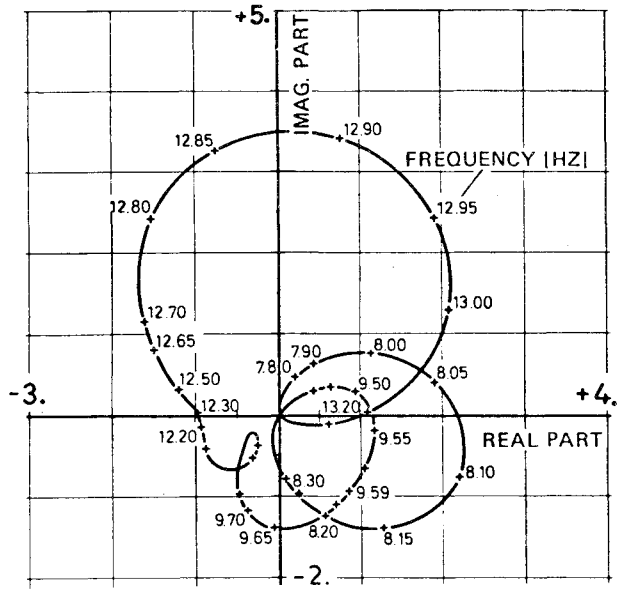

Fig. 8 Open-loop diagram of the roll axis at zero airspeed (roll gyro rate signal).

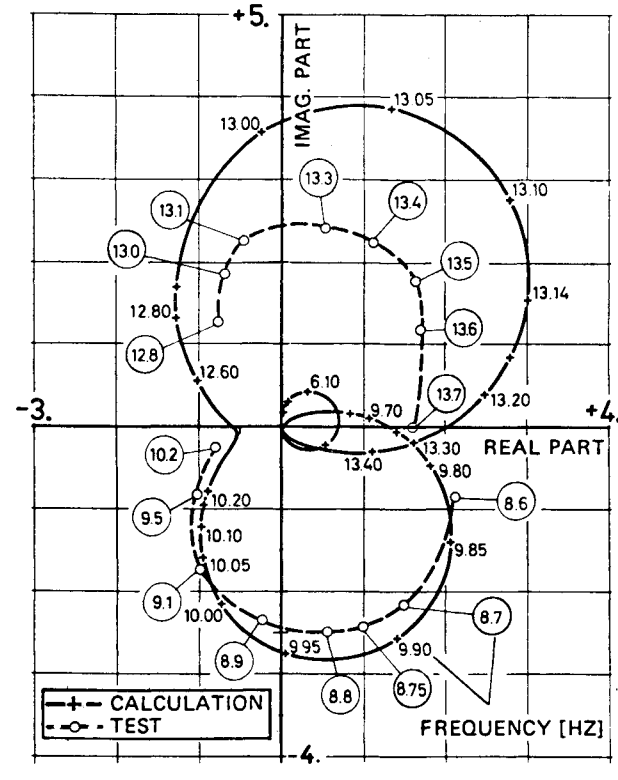

Fig. 7 Open-loop diagram of the pitch axis at zero airspeed (pitch gyro rate signal).

CSAS Structural Mode Coupling Test on the Aircraft

Open-loop tests were conducted with the aircraft standing on inflated and deflated tires for various fuel conditions and wing sweep angles. The purpose of this test was to measure the transfer function of elastic aircraft with CSAS and close the loops whenever stability was assured. In our case this was only possible for the yaw loop. The pitch and roll loops were unstable. After introducing the lag filter into the actuator circuit, the aircraft was stable but did not fulfill our requirements for safety margins.

Notch filters were implemented into the CSAS and the aircraft was retested. All loops could be closed and closed-loop tests also could be performed. The crucial point of all of this testing is to choose several input amplitudes, thus covering the nonlinearities of the actuators, thereby avoiding any limited amplitude self-excited oscillation and not to exceed any structural or engine osicllation fatigue limits. For this latter reason, test time should be kept short and most of the development work must be done analytically.

Analytical Prediction of Required Notch Filter Characteristics

The Nyquist plot of Fig. 7 comparing test with analytical results for a system without structural mode filters (notch filters) but with the lag filter introduced into the taileron actuator circuit shows good correlation for the pitch axis. The structural model had to be adjusted to reflect the test condition of the aircraft standing on tires, and structural damping $g = 0.02$ was introduced for every vibration mode. Figure 7 shows considerable responses in three symmetrical vibration modes. These three modes are identified by their dominant features: Mode I) first symmetrical wing bending (6.13 Hz), Mode II) first fuselage vertical bending (9.91 Hz), and Mode III) first tailplane symmetrical bending (13.07 Hz). The overestimation of the tailplane first bending response by about 6 db (compared to test results) can be attributed to the fact that the structural damping value for this mode was higher than $g = 0.02$. However, it was felt that the damping could be affected by the service life in such a way that it would be reduced to a minimum of 0.02. For this reason the original assumption of $g = 0.02$ was never changed throughout the calculation, thus also covering the airplane in service. The aircraft is stable because the response does not encircle the point (-1) on the real axis.

An open-loop diagram also is shown in Fig. 8 for the roll axis (yaw loop is closed.). Marginal stability is indicated, because the point (-1) on the real axis is almost reached. Responses for four different antisymmetrical vibration modes are apparent. These four modes are: Mode I) first wing antisymmetrical bending (8.1 Hz), Mode II) first fin bending (9.65 Hz), Mode III) first fuselage lateral bending (12.0 Hz), and Mode IV) first antisymmetrical tailplane bending (12.9 Hz).

Stability Requirements

The phase lag introduced into the low-frequency area by a notch filter was expected to be detrimental to the stability of flight mechanical-CSAS coupled modes. Since this phase lag increases with higher notch filter attenuation, there was the

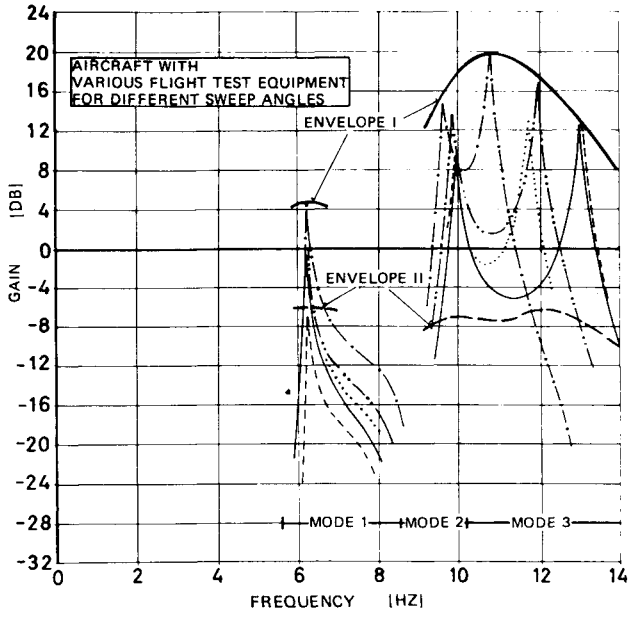

Fig. 9 Structural mode filter layout for the pitch axis (zero airspeed).

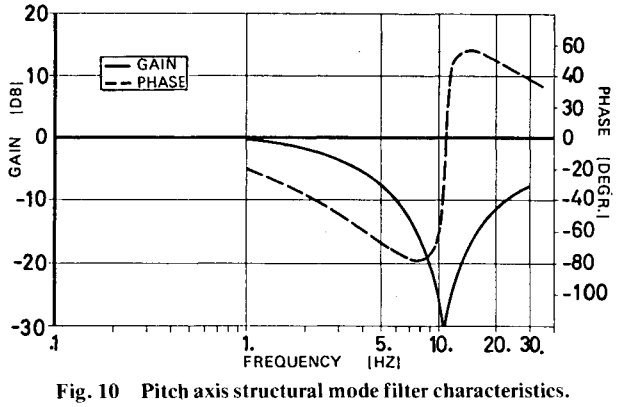

Fig. 10 Pitch axis structural mode filter characteristics.

requirement to keep the attenuation to a minimum. On the other hand, it is necessary to cover frequency and amplitude shifts of structural modes (generated by flight flutter test excitation equipment, wing and fuselage fuel contents, wing sweep), and gain and phase variation of actuators by reasonable margins. It was our opinion, that the requirement for stability of MIL-Spec-A-008870 A§ asking for: "1) a gain margin of at least 6 db, and 2) separately, a phase margin of at least $\pm 60°$" was not conservative enough for our case. We required a 6 db margin on the amplitude of every structural mode and applied MIL-Spec philosophy only for failure cases. As shown by Figs. 7 and 8, this requirement was not satisfied by implementing only a lag filter into the actuator circuit.

How we designed the notch filters is illustrated by Fig. 9. It only demonstrates the procedure for the pitch axis. An analogous procedure was used for the roll axis. Amplitudes of structural mode responses are plotted for various configurations. An envelope is drawn to cover all peaks (Envelope I, Fig. 9). A notch filter is designed that gives at least a 6 db amplitude margin at all frequencies (Envelope II, Fig. 9). Figure 10 shows the pitch notch filter characteristics.

The notch filter for the roll axis has similar properties. The open-loop diagrams for the pitch and roll axes with the notch filters implemented are presented in Figs. 11 and 12, respectively. When comparing these diagrams to Figs. 7 and 8, one must consider the different scales.

§U.S. Air Force, March 31, 1972.

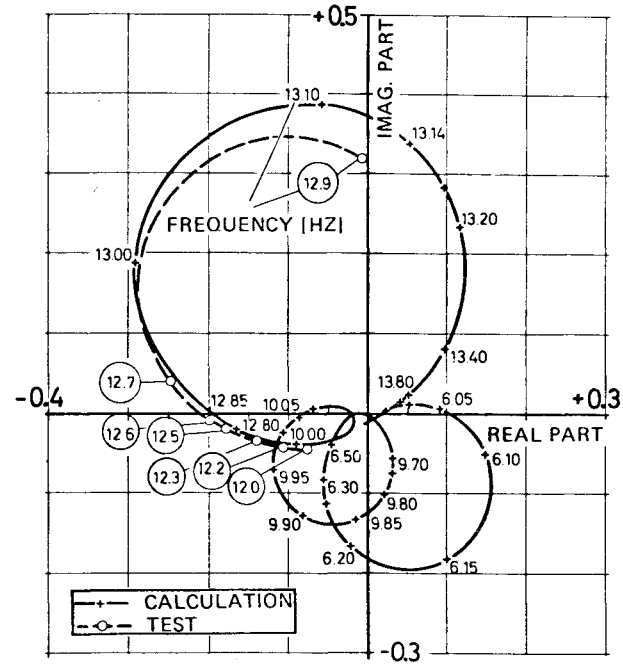

Fig. 11 Open-loop diagram of the pitch axis with notch filter engaged at zero airspeed (pitch gyro rate signal).

Aeroelastic Investigations

One must be sure that no instability can arise in the flight envelope of the aircraft that stems from detrimental coupling of CSAS-structure-unsteady aerodynamic forces. The whole flight envelope must be covered by analyses. At a few velocities flight flutter tests must be conducted.

Unsteady Aerodynamic Forces

The lifting surface method of Ref. 9, including equivalent slope rudder aerodynamics, was used to calculate unsteady aerodynamic forces in the subsonic regime. This method contains interference effects of wing-tail-fin.[10] Pressure distribution measurements were performed which prove the validity of the method.[11]

Supersonic unsteady aerodynamic forces were calculated according to the Mach Box method[12] which was extended to cover wing-tail interference effects.[13]

Results of Analyses Including Unsteady Aerodynamic Forces

Open-loop diagrams of the response of the pitch gyro (notch filter implemented into the CSAS), including the effects of unsteady aerodynamics, are presented in Fig. 13. In comparison with Fig. 11, from this figure one can draw the conclusion that unsteady aerodynamic forces are attenuating. This can be substantiated by the results of Fig. 14 which show *v-g* plots for the augmented and unaugmented free aircraft. Figure 14 shows that the damping of the three important structural modes increases with airspeed. This picture also indicates that there is practically no influence of CSAS on flutter behavior. An analogous investigation was conducted for the roll axis which is not presented here but which gave similar results.

Flight Flutter Test Results

Tests were performed at a few airspeeds with the unaugmented and augmented aircraft by the flight test group of British Aircraft Corporation.[14] First data evaluations show that differences in frequencies and dampings of these two conditions are within measuring accuracy. In Fig. 15 the measured and predicted frequencies and damping vs airspeed are plotted for the most important mode.

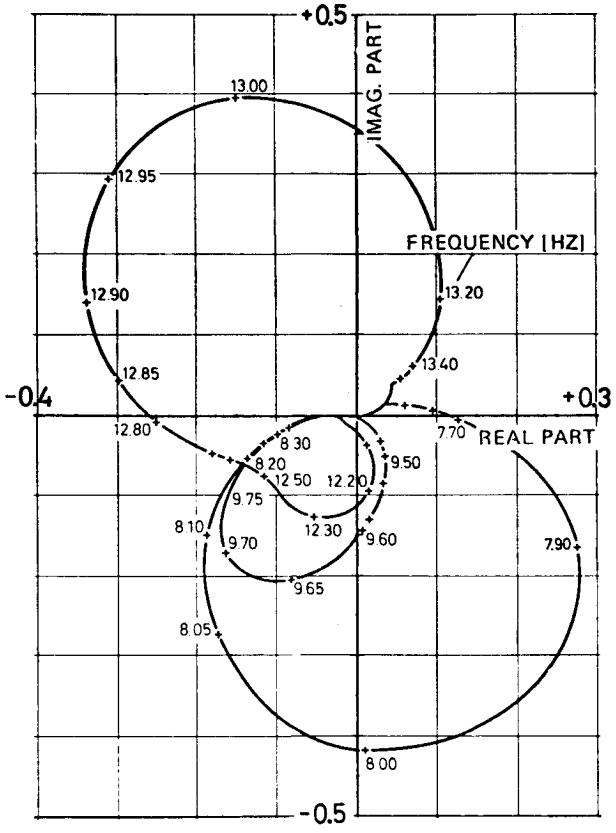

Fig. 12 Open-loop diagram of the roll axis with notch filter engaged at zero airspeed (roll gyro rate signal).

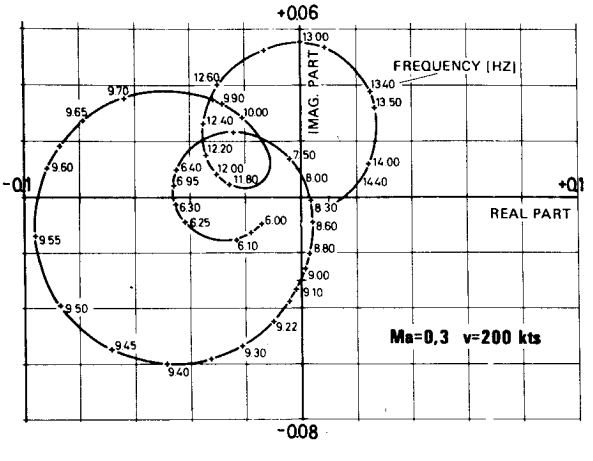

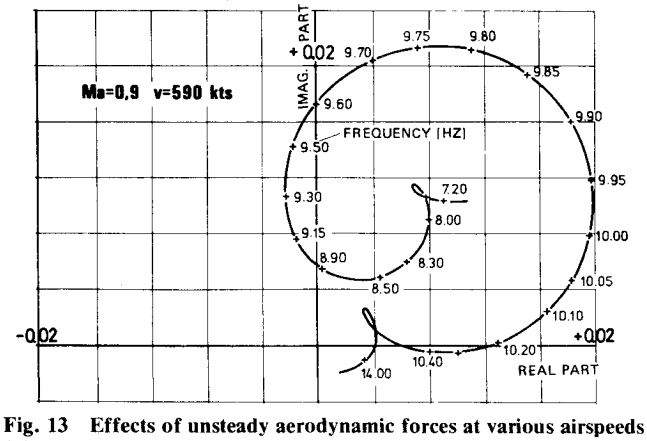

Fig. 13 Effects of unsteady aerodynamic forces at various airspeeds (pitch gyro rate signal).

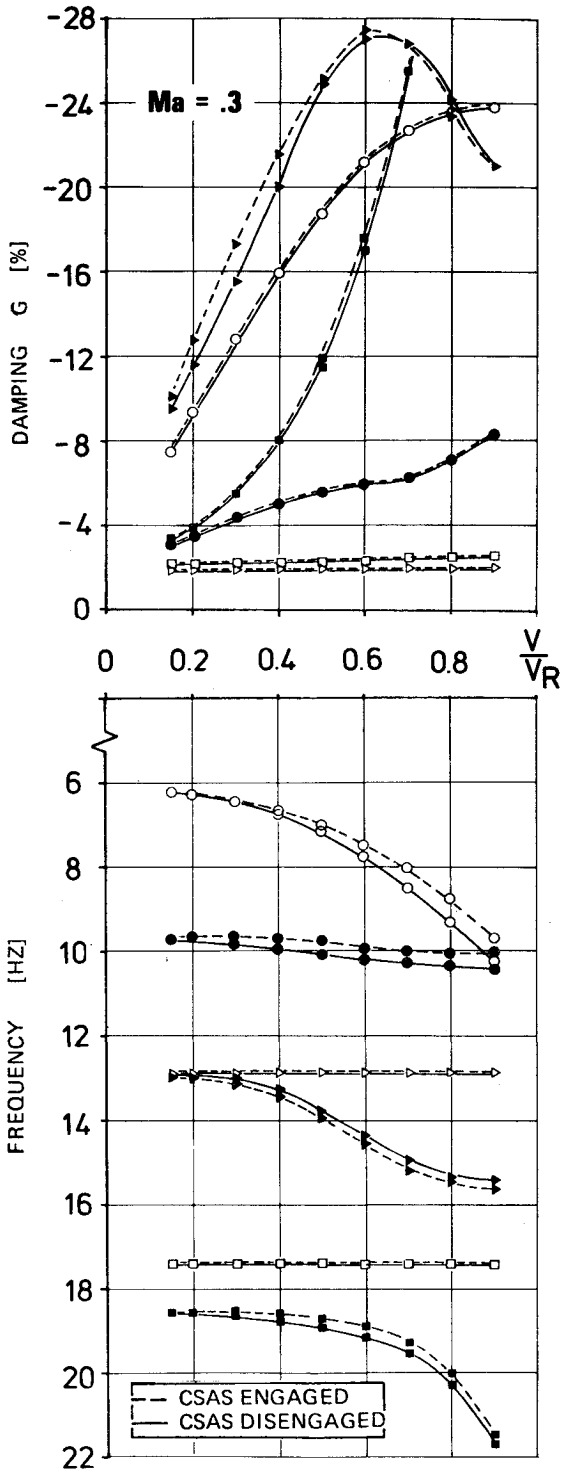

Fig. 14 Closed-loop calculations for the augmented and unaugmented aircraft (pitch axis, $M = 0.3$).

Conclusions and Recommendations

This paper describes experience gained on the Tornado to avoid CSAS-structural mode interaction. The following points should be highlighted:

1) It is absolutely necessary to have a reliable analytical model of the elastic aircraft which must be verified by ground resonance test.

2) Ground tests to check CSAS-structural mode interaction must be performed to assure stability and to compare with analytical predictions. Providing that correlation is achieved, the whole range of variation parameters such as external stores, fuel content, and wing sweep angle can be investigated analytically.

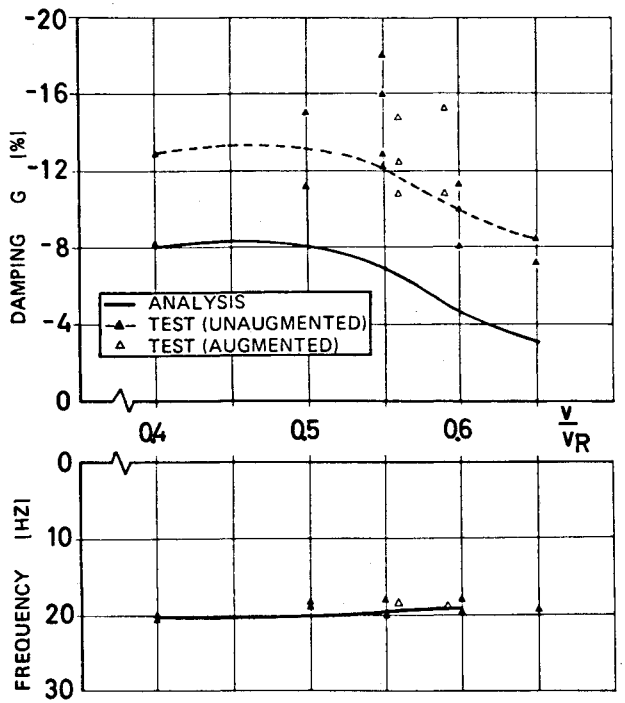

Fig. 15 Comparison of analysis and flight test results (anti-symmetrical taileron mode).

3) Open- and closed-loop calculations must be done to cover the whole flight envelope. Calculations on the Tornado have shown negligible influence of CSAS on flutter behavior. For this reason, only a few test points with the fully operative CSAS had to be flight flutter tested. The calculated trend was proven by the test.

Acknowledgment

The authors wish to acknowledge the cooperative efforts of VFW in contributing the closed-loop analyses results presented here.

References

[1]Haidl, G., Lotze, A., and Sensburg, O., "Active Flutter Suppression on Wings with External Stores," AGARDograph No. 175.

[2]Sensburg, O., Hönlinger, H., and Kühn, M., "Active Control of Empennage Flutter," *AGARD Structures and Materials Panel*, Brussels, April, 13-18, 1975.

[3]Wittmeyer, H., "Flattergleichungen mit Berücksichtigung einer Servosteuerung und eines Flugreglers," *Zeitschrift für Flugwissenschaften*, Vol. 22, 1974, Heft 2.

[4]Försching, H., "Einfluss servomechanischer Steuerungs- und Stabilitätssysteme auf das Flatterverhalten von Flugzeugen," *Zeitschrift für Flugwissenschaften*, Vol. 21, 1973, Heft 1.

[5]Hassig, H.J., "An Approximate True Damping Solution of the Flutter Equation by Determinant Interaction," *Journal of Aircraft*, Vol. 8, Nov. 1971, pp. 885-889.

[6]Sensburg, O., Lotze, A., and Haidl, G., "Wing with Stores Flutter on Variable Sweep Wing Aircraft," *AGARD Conference Proceeding On Wing-With-Stores-Flutter*, No. 162, Munich, Oct. 1974.

[7]Hurty, W.C., "Dynamic Analysis of Structural Systems Using Components Modes," *AIAA Journal*, Vol. 3, April 1965, pp. 678-685.

[8]Lotze, A. and Garr, R., "Eigenschwingungsberechnung statisch unbestimmt verbundener Unterstrukturen mittels dynamischer Kopplung," *Aeroelastik-Kolloquium*, TU Berlin, June 1-2, 1971; also MBB-Rept. UFE 733-71, Messerschmitt-Bölkow-Blohm, 1971.

[9]Laskha, B. and Schmid, H., "Unsteady Aerodynamic Forces on Coplanar Lifting Surfaces in Subsonic Flow (Wing-Horizontal Tail Interference)," *AGARD Structures and Materials Panel Meeting*, Ottawa, Canada, Sept. 25-27 1967.

[10]Sensburg, O. and Laschka, B., "Flutter Induced by Aerodynamic Interference Between Wing and Tail," *Journal of Aircraft*, Vol. 7, Aug. 1970, pp. 319-324.

[11]Becker, J., "Interfering Lifting Surfaces in Unsteady Subsonic Flow (Comparison between Theory and Experiment)," AGARD-Rept No. 614.

[12]Stark, V.J.E., "Calculation of Aerodynamic Forces on Two Oscillating Finite Wings at Low Supersonic Mach Numbers," SAAB TN 53, 1964.

[13]Schmid, H., "A Supersonic Lifting Surface Theory for Predicting Unsteady Interference Airloads on Coplanar Wing-Horizontal Tail Configurations," Messerschmitt-Bölkow-Blohm, MBB-Rept. AN-P-0001, March 1970.

[14]Potter, D.K. "MRCA Flight Flutter Testing," AIAA Aircraft Systems and Technology Meeting, Los Angeles, Calif., 1975.